Statistics of wave-function scars

T. M. Antonsen, Jr.,[1,2] E. Ott,[1,2] Q. Chen,[1] and R. N. Oerter[1,3]
[1]*Laboratory for Plasma Research, University of Maryland, College Park, Maryland 20742*
[2]*Department of Electrical Engineering and Department of Physics, University of Maryland, College Park, Maryland 20742*
[3]*Department of Physics, Howard University, Washington, D.C. 20059*
(Received 22 June 1994)

The properties of "scars" on eigenfunctions (i.e., enhancements along unstable classical periodic orbits) of a two-dimensional, classically chaotic billiard are studied. It is shown that the tendency for a scar to form is controlled by both the stability of the periodic orbit and the statistical fluctuations in the time for wave density to return to the unstable orbit once having left. Both scars and "antiscars" are predicted to occur depending on the nearness of the eigenvalue of the chaotic eigenfunction in question to a value that quantizes the periodic orbit. The theoretical predictions are compared with direct numerical solutions for a bowtie shaped billiard.

PACS number(s): 05.45.+b, 03.65.Ge, 03.65.Sq

I. INTRODUCTION

The properties of semiclassical eigenfunctions of wave equations when the corresponding classical dynamics is chaotic are important in a variety of fields of scientific research. Some time ago Berry proposed that, locally, the eigenfunctions appear to be a superposition of WKB solutions with random phases and amplitudes [1] distributed such that the classical microcanonical ensemble is recovered [2]. In the case of solutions of the two-dimensional Helmholtz equation, $\Delta\Psi+k^2\Psi=0$ with $\Delta\equiv\partial^2/\partial x^2+\partial^2/\partial y^2$ and $\Psi=0$ on the boundary, this leads to the expectation [1] that wave functions in the semiclassical regime will locally appear to be a superposition of plane waves:

$$\Psi=\lim_{N\to\infty}\sqrt{(2/AN)}\,\mathrm{Re}\left\{\sum_{j=1}^{N}a_j\exp(i\alpha_j+i\mathbf{k}_j\cdot\mathbf{x})\right\}, \quad (1)$$

where A is the area of the connected region under consideration, the amplitudes a_j are real positive random numbers whose mean squared value is 1, the phases α_j are randomly distributed on an interval of 2π, and the wave vectors $\mathbf{k}_j$ are uniformly distributed on a circle in $\mathbf{k}$ space with $|\mathbf{k}_j|=k$. The factor $\sqrt{(2/AN)}$ in (1) normalizes the wave function so that $\int_A|\psi|^2dx\,dy=1$.

Due to the fact that the wave function (1) is composed of a superposition of a large number of random variables, the distribution of the values of the wave function was predicted by Berry [1] to be a Gaussian with zero mean and a variance inversely proportional to the area A of the region. This prediction was tested numerically by McDonald and Kaufman [3,4] for a stadium shaped boundary, and they found that it was nearly true for most eigenfunctions but that there were exceptions. In particular, Heller [5] showed that occurrences of excessive concentrations of eigenfunctions on domains corresponding to unstable classical periodic orbits were necessary. He did this by showing that a superposition of chaotic eigenfunctions of the form (1) could not describe the initial propagation and spreading of a wave packet along a weakly unstable periodic orbit. Heller named these concentrations "scars," and their study has been the subject of much recent interest.

As mentioned, Heller's result [5] is based on consideration of the initial spreading of a wave packet; that is, for a time longer than the spreading time determined by the classical stability of the periodic orbit, but shorter than the recurrence time associated with the separation in frequency of adjacent eigenfunctions. As such, his result applies to a superposition of a large number of eigenfunctions and does not determine the degree to which individual eigenfunctions are scarred. Similarly, the theories of Bogomolny [6] and of Berry [7] on fluctuations of the wave-function density based on Gutzwiller's [8] periodic orbit formula also describe the average properties of a large number of eigenfunctions in a classically small energy range. All of these theories have shown that the strength of scarring depends on the stability of the periodic orbit through its Lyapunov exponent.

Subsequent work [9–11] has pursued the approach based on summations over periodic orbits. Efforts have centered on decreasing the classically small energy range of Refs. [6] and [7] to zero in order to arrive at the properties of single eigenfunctions [10]. Ultimately, this requires summing over a large number of periodic orbits, the length (and number) of which increase as the energy averaging range is made smaller. Thus, for detailed answers, the approach becomes computationally intensive.

In this paper, we will discuss the *statistics* of scars on individual eigenfunctions. We will show that the properties of scars can be described as a natural extension of the chaotic eigenfunction picture leading to Eq. (7) below. Our first step is to define a quantitative measure of the degree to which an eigenfunction is scarred by a periodic orbit. In the theories of Bogomolny [6] and Berry [7] the quantity of interest is the wave-function spatial probability density [6] or the phase space density [7] (the Wigner function). These can be compared with the corresponding expected classical value based on the microcanonical

ensemble.

We will consider another quantity V_p (to be defined in Sec. II), which is the projection of the wave function along the periodic orbit on to a plane wave which quantizes the orbit. This quantity will have a value which varies erratically from individual wave function to wave function. A particularly large value will signal the presence of a scar. We will investigate the variations of V_p both numerically and analytically for a specific example of a chaotic billiard problem.

The goal of our analysis is not to derive a formula which when evaluated gives the numerical value of V_p for a particular eigenfunction. This requires, essentially, solution of the wave equation for each eigenfunction. Rather, our principal result is a formula [Eq. (8)] showing that the eigenfunction to eigenfunction variations in the strength of a scar as measured by V_p on a particular periodic orbit can be modeled as a Gaussian random variable with zero mean and a variance that can be easily determined. The tendency to form a scar depends on two factors: one "deterministic" and one "statistical." The deterministic factor (which gives the variance of our model random variable) depends on the closeness of the eigenvalue of the eigenfunction in question to quantizing the given periodic orbit. This factor is larger when the instability of the periodic orbit is weaker. The statistical factor is essentially the time for wave density to return to the vicinity of the unstable periodic orbit once having left. The latter quantity varies erratically from eigenfunction to eigenfunction and is characterized by a probability distribution function.

Strictly speaking, our results are limited to solutions of the two-dimensional Helmholtz equation in the bowtie shaped region of Fig. 1, but we believe that they are, in fact, more general.

The organization of our paper is as follows. In Sec. II we introduce the variable V_p which will give a quantitative measure of the degree to which an eigenfunction is scarred by a periodic orbit. We will first calculate the properties of this variable under the assumption that the wave function is described by Eq. (1). This gives a point of reference for comparison with our subsequent analytic and numerical results. Second, we will present an analytic formula giving the properties of V_p for eigenfunctions. Section III presents the results of a numerical study which confirms to some degree our picture of scars. Section IV presents the detailed mathematical steps by which the results of Sec. II were obtained. Finally, in Sec. V we give some conclusions and speculations.

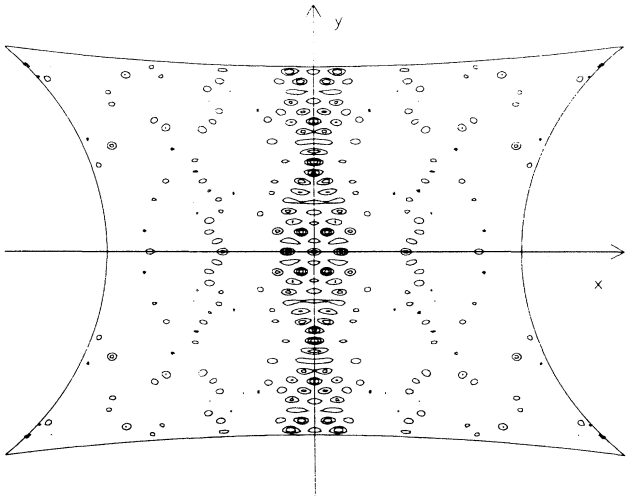

FIG. 1. The bowtie billiard along with the square of the magnitude of the wave function for an eigenfunction which exhibits a scar on the periodic orbit bouncing back and forth between the upper and lower boundaries.

II. SCARS

The chaotic wave function described by Eq. (1), despite being the sum of a large number of independent waves, still exhibits a degree of long range coherence as was pointed out by O'Connor *et al.* [12]. Consider the variable,

$$V_p=\int_{-L/2}^{L/2}\Psi(\mathbf{x})\cos(k_p l)dl\ , \tag{2}$$

where the integral is taken along a straight line of length L, and k_p is a constant ($\hbar k_p$ is the momentum component along the line). If $\Psi(\mathbf{x})$ is a chaotic eigenfunction described by Eq. (1), then V_p is a Gaussian random variable with zero mean and a variance given by

$$\langle V_p^2\rangle_r=[1/(2\pi A)]\int_0^{2\pi}[F_+(\theta)+F_-(\theta)]^2 d\theta\ , \tag{3}$$

where

$$F_\pm(\theta)=\sin[(k\cos\theta\pm k_p)L/2]/(k\cos\theta\pm k_p)\ .$$

Here the subscript r on $\langle V_p^2\rangle_r$ signifies that the result for $\langle V_p^2\rangle$ is from the random plane wave hypothesis Eq. (1). To obtain (3), substitute (1) in (2), square the result, average over the independent random variables a_j and α_j, perform the integrations over l, and pass to the limit $N\to\infty$ (thus producing the integration over the angle θ). If kL and k_pL are large and $|(k-k_p)L|\gg 1$, the main contributions to the integral in Eq. (3) come from the vicinity of the θ values satisfying $k\cos\theta\pm k_p=0$. In this limit we obtain

$$\langle V_p^2\rangle_r\cong L/(A\sqrt{k^2-k_p^2})\ , \tag{4}$$

where use has been made of the integral $\int_{-\infty}^{+\infty}\xi^{-2}\sin^2\xi\, d\xi=\pi$. Thus, in the limit that kL, k_pL, and $|(k-k_p)L|$ are large, the expression (3) for the variance exhibits a square root singularity as k_p approaches k. The square root singularity in Eq. (4) can be seen to result from the projection of the semiclassical Wigner function, which is uniform on a circle of radius k in wave-number space, onto a single axis parallel to the line along which the integral in (2) is carried out. This is illustrated in Fig. 2 for the case in which the line is parallel to the y axis.

Equation (4) is only an asymptotic evaluation of the integral, Eq. (3), giving $\langle V_p^2\rangle_r$. It breaks down when $(k-k_p)L\simeq 1$. Reevaluating the integral in Eq. (3) for kL

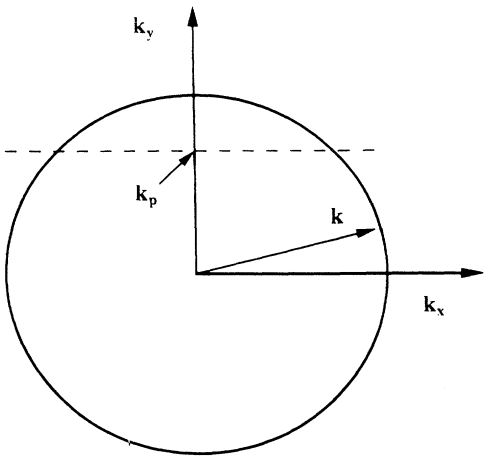

FIG. 2. Wave-number space for a wave function with wave vectors uniformly distributed on a circle of radius k. The dashed line illustrates the projection process by which V_p is obtained.

and k_pL large but $(k-k_p)L \simeq 1$ reveals that the apparent singularity in (4) is cut off. In this case, in the vicinity of $k_p \pm k\cos\theta = 0$, we can use the approximations

$$k_p - k\cos\theta \cong (k_p - k) + k\theta^2/2$$

and

$$k_p + k\cos\theta \cong (k_p - k) + k(\theta - \pi)^2/2 \ .$$

One then obtains from Eq. (3)

$$\langle V_p^2 \rangle_r \cong L^2 G(\lambda)/(A\sqrt{kL}) \ , \tag{5}$$

where

$$G(\lambda) = \int_{-\infty}^{\infty} (\lambda/4 - \zeta^2)^{-2} \sin^2(\lambda/4 - \zeta^2) d\zeta/(2\pi) \ , \tag{6a}$$

$$\lambda = 2(k - k_p)L \ . \tag{6b}$$

Note that as $\lambda \to \infty$ Eqs. (5) and (4) match, as they must.

In terms of Fig. 2, we note that, due to the finite length L of the line, the projection process yielding V_p^2 has a minimum resolution of order L^{-1}. This finite resolution becomes important as k_p approaches k and the dashed line in Fig. 2 becomes tangent to the circle representing the Wigner function. Further, as k_p approaches k, V_p measures the "overlap" between the wave function Ψ and a plane wave propagating along the line.

Equation (5) predicts that the greater the length of the line, the larger the variance of V_p. However, Eq. (5) cannot hold if the length of the line approaches the size of the region in which the eigenfunctions are determined. This is because (1) only describes the local properties of the eigenfunction and does not account for properties at larger scale that are determined by the details of the shape of the boundary. We will now argue that, if the straight line is made to be a periodic orbit, then the eigenfunction to eigenfunction variations of V_p will appear to be a Gaussian random variable with a variance described by Eq. (5) in the important range $(k - k_p)L \approx 1$, but with the function $G(\lambda)$ determining the cutoff of the square root singularity in (2) replaced by another function involving the length of the periodic orbit and its Lyapunov number.

Our particular result applies to the bowtie shaped region depicted in Fig. 1. Due to the negative curvature of the boundary, the classical orbitals of the system are chaotic. We focus on a particular unstable orbit, namely, the orbit that bounces back and forth between the upper and lower boundaries at the center of the bowtie. This orbit is only weakly unstable when the radii of curvature of the upper and lower boundaries are large. We again consider the variable

$$V_p = \int_{-L/2}^{L/2} \Psi_k(0,y) \cos(k_p y) dy \ , \tag{7}$$

where, now $k_p = p\pi/L$, p is an odd integer. L is the separation of the two boundaries at $x = 0$, and Ψ_k is a normalized eigenfunction with eigenvalue k for the Helmholtz equation $\nabla^2\Psi_k + k^2\Psi_k = 0$. The value of V_p defined in this way will vary from eigenfunction to eigenfunction. A particularly large value of V_p signals the presence of a scar since this implies Ψ_k has a large Fourier component which quantizes the orbit. Our analysis (to be presented in subsequent sections) indicates that the eigenfunction to eigenfunction variations of V_p may be modeled as different realizations of a random variable,

$$V_p^2 = \nu^2 L^2 G_1(\lambda_1, \Lambda)/(A\sqrt{kL}) \ , \tag{8}$$

where ν is a Gaussian random variable with zero mean and unit variance. The form factor G_1,

$$G_1(\lambda_1, \Lambda) = 2(\Lambda - 1)^{-1/2} |\partial U_+(\lambda_1, \xi)/\partial\xi|_{\xi=0}^{-2} \ , \tag{9}$$

depends on the nearness of the eigenvalue k to k_p through the variable

$$\lambda_1 = (k^2 - k_p^2)L/[k(\Lambda - 1)] \ , \tag{10}$$

and

$$U_+(\lambda_1, \xi) = \exp[-\pi(\lambda_1 + i/2)/4] \times U(-i\lambda_1, \exp[-i\pi/4]\xi) \ ,$$

where $U(a,z)$ is the parabolic cylinder function defined in Ref. [13]. Here $\Lambda = 1 + \sqrt{8L/R_c}$ is the stability index (Lyapunov number) for the periodic orbit and R_c is the radius of curvature of the upper and lower boundaries. We note that, similarly to Eq. (5) for the chaotic eigenfunction, Eq. (8) agrees with Eq. (4) (apart from a factor of 4) if the asymptotic limit of G_1 is taken for large λ_1, $G_1 \simeq 4\sqrt{k/[L(k^2 - k_p^2)]}$.

The extra factor of 4 in G_1 is due to the even symmetry of the wave function about the x and y axes. This symmetry was used in the derivation of G_1 (Sec. IV), but not in the derivation of the expression for G [Eq. (6)]. The large argument expansion for Eq. (5) can be brought into agreement with that of Eq. (8) by constraining the chaotic eigenfunction (1) to have even symmetry about the x and

y axes [i.e., on the periodic orbit, replace the summand in (1) by $a_j \cos k_{xj} x \cos k_{yj} x$ with the appropriate normalization factor]. Henceforth we insert the factor of 4 where appropriate by defining the new function

$$G_s(\lambda) = 4G(\lambda) ,$$

which applies to the symmetric random eigenfunction. the corresponding version of Eq. (5) has G replaced by G_s.

The analysis giving rise to Eq. (8) leads to the following physical interpretation. A scar will appear on the periodic orbit (measured by the tendency of V_p^2 to exceed $\langle V_p^2 \rangle_r$) if either the time for waves to escape the periodic orbit is large (as determined by the factor G_1/G_s) or the time for waves to return, once having left, is short (as determined by the Gaussian random variable ν). The ratio

$$\langle V_p^2 \rangle / \langle V_p^2 \rangle_r = G_1(\lambda_1, \Lambda)/G_s(\lambda) , \tag{11}$$

gives the expected enhancement of V_p^2 over the random plane wave prediction $\langle V_p^2 \rangle_r$, and gives a measure of the tendency for a scar to form.

The difference between the predictions of Eqs. (5) and (8) for the variance of V_p concerns the way in which the square root singularity in Eq. (3) is cut off as k approaches k_p. In both cases, the cutoff occurs when the difference of the two wave numbers is the inverse of a length. In the case of Eq. (5) (which only applies for sufficiently short lines), the cutoff [occurring at $\lambda \sim 1$; cf. Eq. (6)] is determined by the length of the line; and in the case of Eq. (8), the cutoff [occurring at $\lambda_1 \sim 1$; cf. Eq. (10)] is determined by the classical exponential length of the unstable orbit [14]. Thus for weakly unstable orbits (i.e., Λ just slightly greater than 1) the cutoff of the square root singularity occurs at higher values for G_1 than for G_s. Hence, for p values in the cutoff range, the values of V_p on weakly unstable orbits tend to be larger than would be expected from the random eigenfunction hypothesis, i.e., there are scars.

In the small wavelength limit there will be many eigenfunctions [$O(kA/L)$] whose eigenvalues fall in the range where the predictions of Eqs. (5) and (8) for the variance of V_p differ significantly. This coupled with the knowledge that ν is a Gaussian random variable allows one to make detailed predictions of the number of eigenfunctions which are scarred.

III. NUMERICAL TEST

To test our ideas, we have numerically solved for the eigenvalues and eigenfunctions for the bowtie billiard (restricted to even symmetry about the x and y axes) using the same technique as McDonald [4].

Two different bowtie billiards, corresponding to different dimensions and radii of curvature of the sides, were considered in detail. These are shown in Table I. For each billiard we calculated about 500 eigenfunctions corresponding to the 200th to 700th eigenvalue. Further, we have calculated the scar strength V_p for several different periodic orbits, and about 30 different k_p values, for each orbit and eigenfunction.

TABLE I. Billiard dimensions.

Billiard	A	B
L_y	2.0	2.0
L_x	2.0	2.0
R_y	1.5	4.0
R_x	10.0	2.0
A	4.677 120	4.764 292

We first examine the distribution of V_p values. We note that in the asymptotic range $(k-k_p)L \gg 1$, where Eq. (4) is expected to apply, the quantity $V_p(k^2-k_p^2)^{1/4}$ is by (4) anticipated to have a Gaussian distribution. This assumption is tested in Fig. 3 where we have made a histogram of $V_p(k^2-k_p^2)^{1/4}$ values for the vertical line placed on the periodic orbit at $x=0$, for the billiard shape labeled A in Table I. Also shown in this plot is a Gaussian fit to the data. The measured variance of the data is $\sigma = 1.27$ compared with the theoretical value of $\sigma_{\text{th}} = 1.31$ based on Eq. (4) and the known dimensions of the billiard. For the example shown here the Gaussian prediction appears quite accurate.

Most of the V_p values contributing to the histogram of Fig. 3 are for values of k_p such that $(k-k_p)L \gg 1$ so that Eq. (4) applies and the form of the cutoff for $k \simeq k_p$ is not resolved. To investigate the cutoff, we plot in Fig. 4 a histogram of the average value of $\sqrt{k}\, V_p^2$ versus $\lambda_1 = (k^2-k_p^2)L/[k(\Lambda-1)]$. This is done by assigning the value of V_p for each eigenfunction and k_p value to one of 50 bins based on the corresponding value of λ_1. Only data points for which $-5 < \lambda_1 < 15$, that is, in the cutoff region, are included in this process. The average value of $\sqrt{k}\, V_p^2$ for each bin is computed and plotted. According to Eq. (8) the histogram should approach $L^{3/2} G_1(\lambda_1, \Lambda)/A$ which we have plotted as a solid curve in Fig. 4. Also shown on Fig. 4 as a dashed curve is the random plane wave cutoff function $L^{3/2} G_s(\lambda)/A$ where $G_s = 4G$ and G and λ are defined in Eqs. (5) and (6). This is the result that would be expected if the random plane

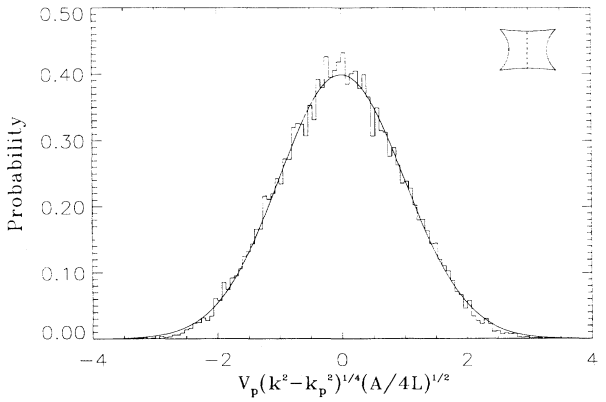

FIG. 3. Histogram of $V_p(k^2-k_p^2)^{1/4}(A/4L)^{1/2}$ values for the vertical periodic orbit at $x=0$ for billiard A of Table I.

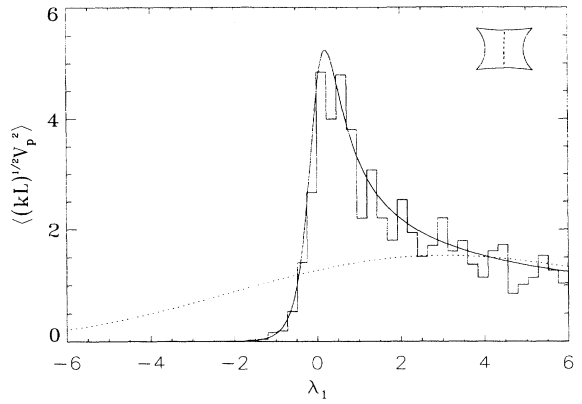

FIG. 4. Histogram of average values of $\sqrt{kL}\,V_p^2$ versus λ_1 for the same case as Fig. 3. Also shown are the theoretical prediction of Eq. (8) as a solid line and the prediction of Eq. (5) as a dashed line.

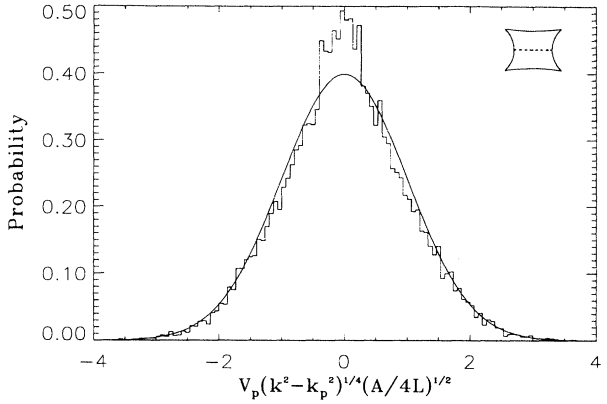

FIG. 6. Histogram of $V_p(k^2-k_p^2)^{1/4}(A/4L)^{1/2}$ values for the horizontal orbit at $y=0$ for billiard A of Table I.

wave hypothesis applied. As can be seen, the shape of the histogram reproduces the function G_1 which is considerably more peaked than the random plane wave cutoff function G_s. The same binning procedure is used in Fig. 5 where we plot a histogram of the average of $V_p^2(k^2-k_p^2)^{1/2}A/4L$ separated into 40 bins based on the value of k_p/k. According to Eq. (4) the value of the histogram in each bin should approach unity. This reflects the uniformity of the Wigner distribution around the circle in Fig. 2. The theoretical and numerical values agree quite closely.

Similar studies were made for the periodic orbit which bounces back and forth along the line $y=0$ in billiard A. The $V_p(k^2-k_p^2)^{1/4}$ and cutoff histograms are shown for this orbit in Figs. 6 and 7. The agreement for this orbit is not as good as in the case of the vertical orbit. In particular, the $V_p(k^2-k_p^2)^{1/4}$ histogram shows an anomalous concentration of small V_p values. One possible cause of this discrepancy is that the radius of curvature of the top and bottom of this billiard is too large and the resulting classical orbits are not sufficiently chaotic. This hypothesis is supported by the results of billiard B of Table I in which both radii or curvature are large. Shown in Figs. 8(a)–8(c) are histograms of $V_p(k^2-k_p^2)^{1/4}$ for (a) the vertical orbit at $x=0$, (b) the horizontal periodic orbit at $y=0$, and (c) the diamond shaped orbit shown with a scarred eigenfunction in Fig. 9.

For the diamond shaped orbit of Fig. 9 we must generalize our definition of V_p for an orbit which does not retrace itself. In addition, it is necessary to account for the vanishing of the wave function at the boundary of the billiard. Close to the boundary the wave function can be thought of as the sum of an incident and reflected wave. The condition $\Psi=0$ at the boundary implies that the reflected wave has the same amplitude as the incident wave but has a phase shift of π. As a result we define

$$V_p=\tfrac{1}{2}\int_0^{L_T}\Psi(l)\sin(k_p l+n\pi)dl\ ,$$

where L_T is the total length of the orbit, l is the distance

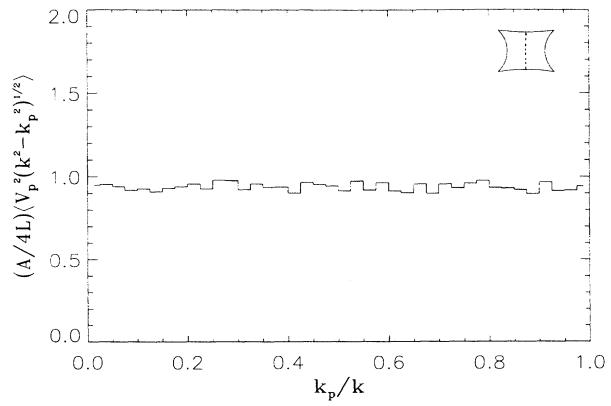

FIG. 5. Histogram of average values of $V_p^2(k^2-k_p^2)^{1/2}A/(4L)$ versus k_p/k for the same case as Fig. 3.

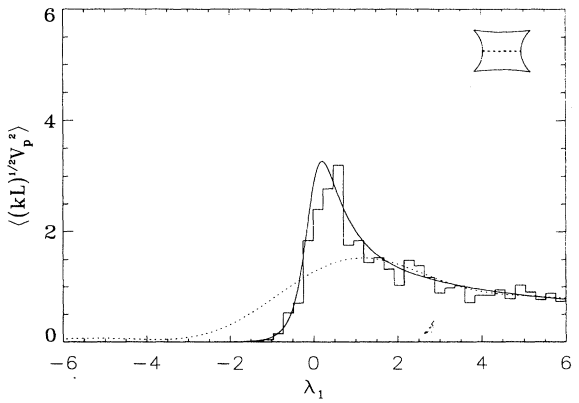

FIG. 7. Histogram of average values of $\sqrt{kL}\,V_p^2$ versus λ_1 for the same case as Fig. 6. Also shown are the theoretical prediction of Eq. (8) as a solid line and the prediction of Eq. (5) as a dashed line.

along the orbit starting at some boundary, and n is the number of reflections between the starting point and the point l. The k_p are quantized according to

$$k_p L_T + N\pi = p\pi \ ,$$

where N is the total number of reflections along the orbit. The factor of $\frac{1}{2}$ in the definition guarantees that the expression for V_p reduces to the previous definition for the back and forth orbits considered previously.

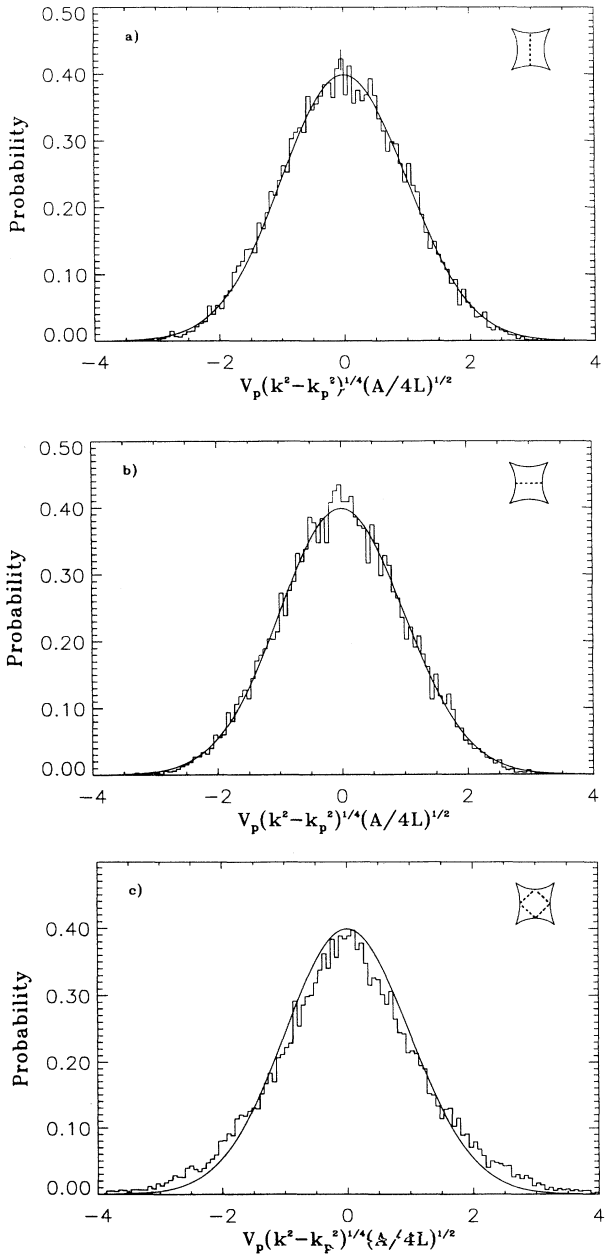

FIG. 8. Histograms of $V_p(k^2-k_p^2)^{1/4}(A/4L)^{1/2}$ values for three periodic orbits in billiard B of Table I: (a) the vertical orbit at $x=0$, (b) the horizontal orbit at $y=0$, and (c) the diamond shaped orbit of Fig. 9.

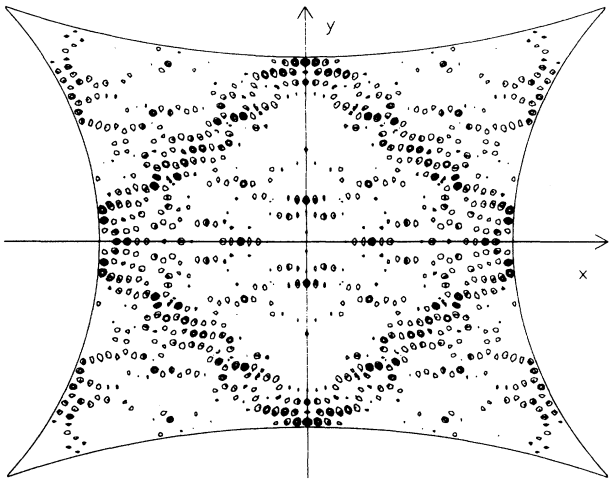

FIG. 9. A scar on the diamond shaped orbit of billiard B.

For the diamond shaped orbit and in the case of wave functions with symmetry in both x and y, the only nonvanishing amplitudes occur for $k_p = 4\pi p/L_T$ ($p=1,2,3,\ldots$). The definition for V_p is then equivalent to

$$V_p = 2\int_0^{L_T/4} \Psi(l)\sin(k_p l)dl \ ,$$

where the integral is carried out along one of the four legs of the orbit. Since the wave functions are no longer symmetric with respect to reflection about the orbit the expected values of V_p^2 should only be enhanced by a factor of 2 as opposed to a factor of 4 for the back and forth orbits. Thus for the diamond orbit Eq. (4) should read

$$\langle V_p^2 \rangle_r = \frac{2L_T}{A\sqrt{k^2-k_p^2}} \ .$$

Similar modifications apply to Eqs. (5) and (8).

The histograms shown in Figs. 3, 6, and 8, are constructed using approximately 1.5×10^4 values of V_p. The central bins contain about 460 entries. Thus one expects the fluctuations in the histogram height to be about $\pm1.4\times10^{-2}$. This is indicated by the error bar on Fig. 8(a).

Figure 10 displays the cutoff histograms for the same three orbits as in Fig. 8. Again, the histograms correspond to the prediction of Eq. (8).

In conclusion, the numerical results show that the eigenfunction to eigenfunction variations in V_p can be modeled as a Gaussian random variable with zero mean. The variance of V_p appears to be given by Eq. (4) if the wave number k_p and eigenvalue k are sufficiently different. The variance is given by Eq. (8) if k_p and k are close to one another. The expected value of V_p^2 is enhanced in this latter case if the relevant periodic orbit is weakly unstable. This enhancement signals the presence of a scar.

IV. ANALYSIS

We now describe the mathematical steps by which Eq. (8) is obtained. We first expand the wave function and its derivative with respect to x in a Fourier series in y,

$$\Psi(x,y)=(2/L)\sum_p V_p(x)\cos[k_p(x)y] , \tag{12a}$$

$$\partial\Psi/\partial x=(2i/L)\sum_p I_p(x)\cos[k_p(x)y] , \tag{12b}$$

where $k_p(x)=p\pi/L(x)$, p is an odd integer, and $L(x)$ is the vertical width of the bowtie billiard at x. Here we have assumed the wave function is even in y. Such an expansion makes sense as long as one restricts x to values such that $|x|<L_x$, where L_x is the distance from the center of the bowtie to the curved side walls. Inserting Eqs. (12a) and (12b) into the Helmholtz equation, and projecting out various Fourier components, results in the following set of differential equations for the coefficients $I_p(x)$ and $V_p(x)$:

$$\frac{\partial}{\partial x}V_p(x)+\sum_{p'}\kappa_{pp'}V_{p'}=iI_p , \tag{13a}$$

$$\frac{\partial}{\partial x}I_p+\sum_{p'}\kappa_{pp'}I_p=i[k^2-k_p^2(x)]V_p , \tag{13b}$$

where

$$\kappa_{pp'}(x)=2\int_{-L/2}^{L/2}dy\,\cos k_p y\frac{\partial}{\partial x}\{L^{-1}(x)\cos[k_{p'}(x)y]\}$$

is a coupling coefficient due to the varying height of the bowtie. Equations (13a) and (13b) are formally the same as those for the voltages and currents on an infinite set of coupled transmission lines. This analogy will be noted at stages of the development. However, it is not essential to following the derivation.

We now imagine partitioning space into a small "inner" region surrounding the periodic orbit and an "outer" region, namely, the rest of the billiard. For small x (i.e., near the periodic at $x=0$) and assuming the orbit is weakly unstable (R_c/L is large), we can neglect in Eq. (13) the coefficient $\kappa_{p'p}$ which couples "voltages" and "currents" on different transmission lines (i.e., $p\neq p'$). The precise conditions under which this is permissible will be given subsequently. The result is that the "voltage" $V_p(x)$ satisfies a Weber equation near the periodic orbit at $x=0$,

$$V_p''(x)+(k^2-k_p^2(0)\{1-2x^2/[R_cL(0)]\})V_p(x)=0 , \tag{14}$$

which follows from an expansion of $k_p(x)$ in Eq. (13b) for small x,

$$k_p(x)\simeq k_p(0)\{1-x^2/[R_cL(0)]\} .$$

Here the instability of the periodic orbit appears as an effective quadratic potential (an antiwell) produced by the curvature of the boundaries.

Solutions of Eq. (14) can be expressed in terms of parabolic cylinder functions,

$$V_p(x)=c\,\mathrm{Re}\{U_+(\lambda_1,\zeta)+\exp(i\Phi_o)U_+^*(\lambda_1,\zeta)\} , \tag{15}$$

where $\zeta=x/R$, $\lambda_1=R^2(k^2-k_p^2)$, $R^2=\sqrt{R_cL(0)/8k_p^2}$, and

$$U_+(\lambda_1,\zeta)=\exp[-\pi(\lambda_1+i/2)4]\times U(-i\lambda_1,\exp[-i\pi/4]\zeta) ,$$

U_+^* is the complex conjugate of U_+, U is the parabolic cylinder function [12], c is a normalization constant, and we have assumed $k_p\simeq k$.

The quantity $\Phi_o(k^2)$ in the above solution for $V_p(x)$

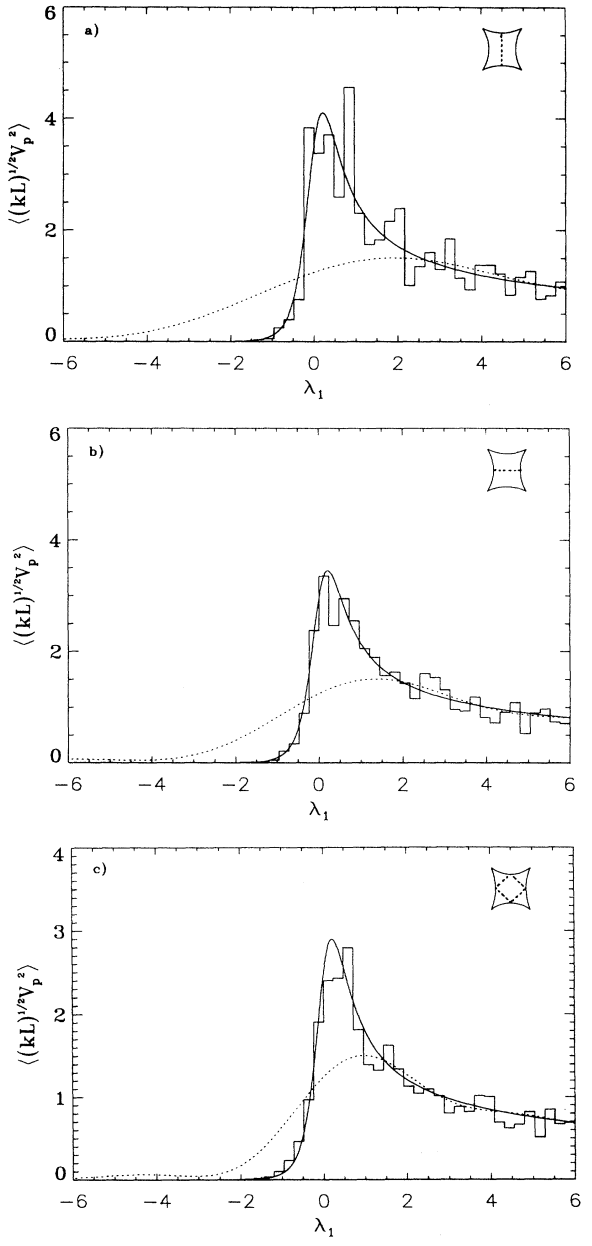

FIG. 10. Histograms of the average values of $\sqrt{kL}\,V_p^2$ versus λ_1 for the same three cases as in Fig. 8.

describes the phase relation between a wave leaving the vicinity of the unstable periodic orbit and one returning. One can think of $\exp(i\Phi_o)$ as the reflection coefficient characterizing the outer region. This is seen by examining the asymptotic form of the solution V_p as $\zeta \to \infty$, in which case

$$U_+(\lambda_1,\zeta) \approx \exp[i\zeta^2/4+(i\lambda_1-\tfrac{1}{2})\ln\zeta]$$

represents an outgoing wave and U_+^* an incoming wave. The behavior of the phase $\Phi_o(k^2)$ depends on the solution of the wave equation away from the periodic orbit. It is through Φ_o that details of the global shape of the boundary influence V_p.

It follows from Eq. (15) and its subsequent definitions that for $k \simeq k_p$ the characteristic scale for variation of the V_p with x is R [which is defined following Eq. (15)]. The assumption that coupling to other Fourier components in Eq. (13) can be neglected will be valid provided that variation of separation between the upper and lower boundaries as x is varied over a distance R is much smaller than a wavelength. Using $L(x) \simeq L(0)+x^2/R_c$, this requires $kR^2/R_c \ll 1$ or $\sqrt{L(0)/8R_c} \ll 1$. Thus the approximation leading to Eq. (14) requires that the orbit be only weakly unstable.

Equation (15) describes the amplitude of the Fourier component of the wave function which quantizes the periodic orbit. Since the orbit is unstable, the effective potential does not confine wave density to the orbit. Rather, wave density spreads away from the orbit where it bounces around the rest of the billiard, eventually returning and interfering constructively or destructively with itself. These processes occurring in the rest of the billiard are described by the phase $\Phi_o(k)$ while the behavior of wave density in the vicinity of the periodic orbit is described by the parabolic cylinder functions.

We would like to extract from Eq. (15) the value of V_p at $x=0$. This requires determination of the normalization constant c. The value of c is determined by the requirement that the square of the wave function when integrated over all area is unity. To determine c we borrow a technique from circuit theory. We imagine that a source is added to the Helmholtz equation,

$$\nabla^2\Psi + k^2\Psi = \frac{2iI}{L}\cos(k_q y)\delta(x) \ . \tag{16}$$

Here the source is localized to the periodic orbit by the δ function and has a sinusoidal variation with wave number k_q along the orbit. The strength of the source is determined by the parameter I which will be likened to a current in the transmission line analogy.

Equation (16) is no longer an eigenvalue equation, and k^2 may be viewed as a continuously adjustable parameter. Equation (16) will be singular if k is chosen to be one of the eigenvalues for the billiard. In this case a vanishingly small current I can produce a nonzero wave eigenfunction Ψ.

The presence of the localized source in Eq. (16) produces a discontinuity in the x derivative of the wave function. That is,

$$\left.\frac{\partial\Psi}{\partial x}\right|_{x=-0}^{x=+0} = \frac{2iI}{L}\cos(k_q y) \ , \tag{17a}$$

or, in terms of voltages and currents defined in Eq. (12),

$$\left.\frac{\partial}{\partial x}V_q\right|_{x=0-}^{x=0+} = iI \ . \tag{17b}$$

The source can be accounted for in the transmission line equations by adding the term $i\delta(x)I\delta_{pq}$ (where δ_{pq} is the Kronecker delta function) to the right-hand side of Eqs. (13b) and (14). This implies that a current source of strength I has been added at $x=0$ to the qth transmission line.

The source will excite a wave function, producing a "voltage" $V_q(0)$ at the location of the source. Since the problem is linear, one can write

$$Y_q(k^2)V_q(0) = I \ , \tag{18}$$

where the constant of proportionality $Y_q(k^2)$ can be thought of as an admittance characterizing the billiard or its transmission line system equivalent.

According to Eqs. (17b) and (18) the admittance is given by the ratio of the jump in the x derivative of V_q to the value of V_q,

$$Y_q(k^2) = \frac{-i}{V_q(0)}\left.\frac{\partial V_q}{\partial x}\right|_{x=0-}^{x=0+} \ . \tag{19}$$

The admittance has several important properties. First, we multiply Eq. (16) by ψ^* and integrate over all of the billiard to obtain

$$\int dx\,dy\,[k^2|\Psi|^2-|\nabla\Psi|^2] = i\frac{2}{L}Y_q(k^2)|V_q(0)|^2 \ . \tag{20}$$

Thus the admittance is imaginary. This is a consequence of the Hermitian property of the Helmholtz equation. In terms of the transmission line analogy, energy is stored on the transmission lines but no power is dissipated, implying an imaginary admittance. Second, if k^2 is selected to be an eigenvalue of the billiard it follows from Eq. (18) that the admittance must vanish. This is because, for an eigenvalue, one has a nonzero V_q in the absence of a source. Finally, we differentiate Eq. (20) with respect to k^2 and evaluate the result for k^2 equal to an eigenvalue and consequently Ψ equal to the corresponding eigenfunction. In performing this differentiation we must differentiate k^2 not only where it appears explicitly, but also where it appears implicitly; for example, in the wave function Ψ and the "voltage" $V_q(0)$. Fortunately, the implicit dependences vanish. Variations of the wave function about an eigenfunction make the left-hand side of Eq. (20) stationary. Further, since the admittance vanishes for an eigenvalue, variations of the voltage on the right-hand side of Eq. (20) do not contribute. The result is

$$\int dx\,dy\,|\Psi|^2 = i\frac{2}{L}\frac{dY_q}{dk^2}|V_q(0)|^2 \ . \tag{21}$$

The transmission line analogy for the preceding is the

statement that the total energy stored in the system is given by the derivative with respect to frequency of the product of the square of the voltage at any port and the reactive admittance.

Now, if we demand that the eigenfunction be normalized to unity we have

$$|V_q(0)|^2=\left[\frac{2i}{L}\frac{dY_q}{dk^2}\right]^{-1} . \tag{22}$$

Thus knowledge of the derivative of the admittance with respect to k^2 gives the value of $V_q(0)$.

To use this relation to determine V_p we take the following steps. With the source, Eq. (14) now has on the right-hand side $iI\delta(x)\delta_{pq}$. Since the source is localized at $x=0$ the solution still has the form of Eq. (15) for $\zeta>0$. For $\zeta<0$ the solution can be obtained by assuming even symmetry. Letting $p=q$, we then have from (19)

$$Y_p(k^2)=-\frac{2i\,\mathrm{Re}\{U'_+(\lambda_1,0)+\exp(i\Phi_o)U^{*'}_+(\lambda_1,0)\}}{R\,\mathrm{Re}\{U_+(\lambda_1,0)+\exp(i\Phi_o)U^{*}_+(\lambda_1,0)\}} , \tag{23}$$

where

$$U'_+(\lambda_1,0)=\partial U'_+(\lambda,\zeta)/\partial\zeta|_{\zeta=0} .$$

The condition for the eigenfunction ($Y_p=0$) is that k^2 should satisfy

$$1+\exp\{i\Phi_o(k^2)+i\Phi_i[\lambda_1(k^2)]\}=0 , \tag{24}$$

where

$$\Phi_i(\lambda_1)=-2\arg[U'_+(\lambda_1,0)] .$$

Here, $\Phi_o(k^2)$ represents the phase of the reflection coefficient attributed to the outer region and $\Phi_i(\lambda_1)$ is the phase attributed to the inner region near the periodic orbit. We note that the dependence of Φ_o on k^2 is much more rapid than that of $\Phi_i(\lambda_1(k^2))$. In particular, adjacent eigenfunctions (with even symmetry in x and y) have a typical separations in k^2 values of $16\pi/A$ (A is the area of the billiard) and correspond to separations of the total phase $\Phi_o+\Phi_i$ of 2π. Since Φ_i depends on k^2 through $\lambda_1=(k^2-k_p^2)L/[k(\Lambda-1)]$ it changes more slowly with k^2 (by a factor of order k^{-1}) than Φ_o does. Thus the separations in k^2 values between adjacent eigenfunctions are determined primarily by the phase of the reflection coefficient characterizing the outer region. A schematic plot of this phase (mod2π) is shown in Fig. 11. The eigenvalues are determined by the intersections of the solid and dashed curves. The spacings between adjacent eigenvalues can be expected to exhibit the characteristic Wigner distribution associated with level repulsion.

Equation (23) provides an expression for the admittance. Differentiation of this expression with respect to k^2 and evaluating the derivative for k^2 equal to an eigenvalue gives

$$\frac{dY_p}{dk^2}=-\frac{2i}{R}|U'_+(\lambda_1,0)|^2\frac{d}{dk^2}[\Phi_o(k^2)+\Phi_i(\lambda_1)] , \tag{25}$$

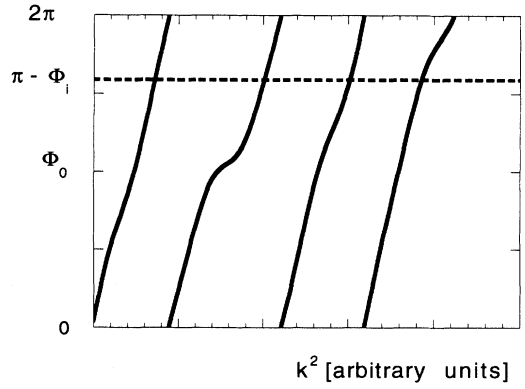

FIG. 11. Schematic representation of the reflection phase $\Phi_o(k^2)$ versus k^2. The dashed curve represents $\pi-\Phi_i$ and the intersection of the solid and dashed curves determine the eigenvalues.

where we have utilized the Wronskian relation $(U'_+U^*_+-U'^*_+U_+)=i$. Since we expect the derivative of the outer phase Φ_o to dominate that of the inner phase Φ_i in Eq. (25), we drop the derivative of the inner phase from Eq. (25). Inserting the expression for dY_p/dk^2 into Eq. (22) (with q set to p) results in Eq. (8), where ν^2 is given by

$$\nu^2=\frac{A}{8}\left[\frac{d\Phi_o(k^2)}{dk^2}\right]^{-1} . \tag{26}$$

We thus see that the variable V_p^2 can be expressed as the product of a form factor $G_1(\lambda_1)$ which varies relatively smoothly with k^2 and a function ν^2 which varies erratically from eigenfunction to eigenfunction (and p value to p value). We argue subsequently that the distribution of ν^2 should be universal.

The quantity ν^2 can be interpreted as follows. The outer region has a reflection coefficient $\exp(i\Phi_o)$. The usual phase delay giving a measure of the time wave density spends in the outer region before returning to $x=0$ with variation $\cos[p\pi y/L(0)]$ is $T_p=\hbar\, d\Phi_o/dE$ ($E=\hbar^2k^2/2m$ is the energy), which, in our normalized units is $T_p=2\,d\Phi_o/dk^2$. Thus $T_p\sim 1/\nu^2$, and we see from Eq. (8) that, as one might guess, V_p^2 is smaller if the wave takes longer to return (i.e., T_p is larger).

If k_j^2 and k_{j+1}^2 are two successive eigenvalues, then it follows from Eq. (24) that $\Phi_o(k_{j+1}^2)-\Phi_o(k_j^2)\cong 2\pi$ for large j. Thus $2\pi(d\Phi_o/dk^2)^{-1}$ is of the order of the spacing between (even) eigenvalues, which in the Weyl approximation has an average of value $16\pi/A$. Hence ν^{-2} can be viewed as a normalization of the erratically varying delay time T_p to its typical value. In terms of Fig. 11 the values of ν^{-2} are determined by the slopes of the Φ_o versus k^2 curve at the points of intersection with the dashed line. We therefore conjecture that these values when appropriately normalized should have a universal distribution, just as the spacings have a universal distribution. This conjecture is supported by our numerical calculations and is reinforced by noting that if ν is a Gaussian random variable the statistical properties of V_p

match those for the random eigenfunction in the asymptotic regime $|k-k_p|L \gg 1$. That is, if v is a Gaussian random variable with the zero mean and unit variance and we evaluate Eq. (8) in the asymptotic regime $\lambda_1 \gg 1$, we recover Eq. (4).

With respect to the numerical calculations shown in Figs. 3, 6, and 8 we note that, to get sufficiently good statistics for the distribution of v, it was necessary to consider a range of k_p values much larger than the cutoff width. We are, however, primarily interested in the statistics of v in the cutoff region. Since the phase $\Phi_o(k^2)$ which determines v^2 characterizes the solution in the outer region, it should not depend on the nearness of k to k_p. Thus the Gaussian result, indicated by Figs. 3, 6, and 8, should apply in the cutoff region as well.

V. DISCUSSION AND CONCLUSIONS

Expressions (8) and (4) allow us to make predictions about eigenfunctions which have scars. For example, one might ask what is the wave density along the periodic orbit. Using Parseval's theorem and the representation (12a) we have

$$P \equiv \int_{-L/2}^{L/2} \frac{dy}{L} |\Psi(x=0,y)|^2 = \frac{2}{L^2} \sum_p |V_p|^2 . \tag{27}$$

According to our theory, each of the V_p in Eq. (27) can be modeled as an independent Gaussian random variable according to Eqs. (8) and (4) depending on the value of λ_1. The variable P is then expected to be a Gaussian random variable with a mean and variance given by

$$\langle P \rangle = 2L^{-2} \sum_p \langle |V_p|^2 \rangle \tag{28a}$$

and

$$\langle (P-\langle P \rangle)^2 \rangle = 4L^{-4} \sum_p [\langle |V_p|^4 \rangle - \langle |V_p|^2 \rangle^2]$$
$$= 8L^{-4} \sum_p \langle |V_p|^2 \rangle^2 . \tag{28b}$$

We consider now the mean value of P in order to compare it with the random plane wave prediction. Taking the difference of the two predictions we have

$$\langle P \rangle - \langle P \rangle_r = 2L^{-2} \sum_p [\langle |V_p|^2 \rangle - \langle |V_p|^2 \rangle_r] . \tag{28c}$$

The expected value of P for the random plane wave case can be obtained directly from Eq. (1), and inserting the previously mentioned factors to account for symmetry $\langle P \rangle_r = 2/A$. To evaluate Eq. (28c) we note that the expressions for $\langle |V_p|^2 \rangle$ and $\langle |V_p|^2 \rangle_r$ are the same in the asymptotic regime $(k-k_p)L \gg 1$. Thus differences that arise in the two predictions result from the cutoff region where Eqs. (8) and (5) apply. This gives

$$\langle P \rangle - \langle P \rangle_r = 2(A\sqrt{kL})^{-1} \sum_p [G_1(\lambda_{1p}) - G_s(\lambda_p)] , \tag{29}$$

where the subscript p emphasizes the p dependence of the λ's. As a function of k, this deviation is nearly periodic with a period π/L. The deviation is positive (a scar) if the eigenfunction has a k value that is close to quantizing the orbit (i.e., $k=k_p$) and is negative (an antiscar) if k is midway between two k_p values. The deviation is largest for weakly unstable orbits and all but disappears as the orbit becomes more unstable.

In Fig. 12 we have plotted a histogram of the averages of the deviation $\sqrt{kL}\,[\langle P \rangle - \langle P \rangle_r]$ for eigenfunctions which are grouped into bins according to their values of $\mu = (k-k_p)L/2\pi$, where k_p is chosen to put μ in the interval $|\mu| \leq 0.5$. This plot is for vertical periodic orbits in billiard A. Also plotted is the predicted value $2\sum_p [G_1(\lambda_{1p}) - G_s(\lambda_p)]/A$ according to Eq. (29). The theoretical curve and numerical data follow roughly the same shape and indicate the tendency for a scar to form if k has a value close to quantizing the periodic orbit $\mu=0$. The error bars show the standard deviation of the data in each bin. The regions of scars and antiscars are clearly seen in the data and conform generally to the theoretical prediction.

It is interesting to compare the wavelength dependences of the various characterizations of the scar strength. First, we note that if one is evaluating the individual values of V_p for a particular periodic orbit and various eigenfunctions, the enhancement in the expected size of those V_p in the cutoff range $(k-k_p)L \sim 1$ persists even as the wave number goes to infinity. This is indicated in Eq. (11).

For a given orbit and eigenfunction, at most one or two values of V_p will fall in the cutoff range $(k-k_p)L \sim 1$ where Eq. (11) appreciably exceeds unity. Any classical observable, such as the orbit averaged density P defined in Eq. (27), will involve a sum over a large number of the V_p's. This dilutes the importance of the one or two in the cutoff region and yields a quantity which approaches the classical value as the wave number goes to infinity. For example, the expected value of P averaged over a large number of eigenfunctions approaches the classical value

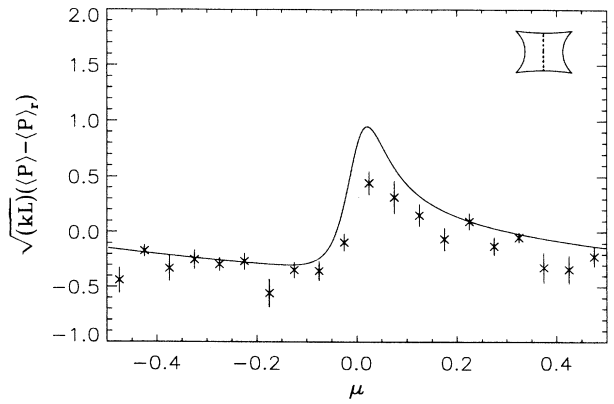

FIG. 12. Deviation between the average wave density on the vertical periodic orbit of billiard A and the corresponding value based on the random eigenfunction hypothesis versus $\mu = (k-k_p)L/2\pi$. The solid curve is the theoretical prediction Eq. (29) and the data points with error bars are the numerical results.

as $k^{-1/2}$ according to Eq. (29). The fluctuations in the values of P for individual eigenfunctions are larger. According to Eq. (28b) and using Eq. (4) for V_p we have

$$\langle (P-\langle P\rangle)^2\rangle \simeq \frac{32}{\pi}\frac{1}{A^2 kL}\ln(kL)\ , \tag{30}$$

which is larger than the fluctuation in the mean given by Eq. (29).

In conclusion, we have obtained a fairly complete picture of the statistical properties of scars in a particular billiard, and we believe that these results can serve as a guide to what should be expected in general. The formation of a scar is controlled by the stability of the periodic orbit in question and the eigenfunction to eigenfunction variations in the time for wave density to return to the vicinity of the periodic orbit after it has left. The latter effect can be modeled as a Gaussian random variable, while the former effect specifies the variance of the Gaussian variable. We have developed an analytic model and tested it by numerical simulation of the wave equation. Agreement between analysis and numerical results is confirmed.

ACKNOWLEDGMENTS

We thank S. Fishman, L. Couchman, and R. Blümel for discussions. This work was supported by the Naval Research Laboratory's Physical Acoustics Center.

[1] M. V. Berry, in *Chaotic Behavior of Deterministic Systems,* Les Houches Lectures XXXVI, edited by G. Loose, R. H. G. Helleman, and R. Stora (North-Holland, Amsterdam, 1983), pp. 171–271.
[2] A. I. Shnirelman, Usp. Mat. Nauk **29**, 181 (1974).
[3] S. W. McDonald and A. N. Kaufman, Phys. Rev. A **37**, 3067 (1988).
[4] S. W. McDonald, Ph.D. thesis, University of California at Berkeley, Lawrence Berkeley Laboratory Report No. 14837, 1983.
[5] E. J. Heller, Phys. Rev. Lett. **53**, 1515 (1984).
[6] E. Bogomolny, Physica D **31**, 169 (1988).
[7] M. V. Berry, Proc. R. Soc. London Ser. A **423**, 219 (1989).
[8] M. G. Gutzwiller, J. Math. Phys. **12**, 343 (1971).
[9] M. V. Berry and J. P. Keating, Proc. R. Soc. London Ser. A **437**, 151 (1992).
[10] O. Agam and S. Fishman, J. Phys. A **26**, 2113 (1993).
[11] M. Feingold, R. G. Littlejohn, S. B. Solina, and J. S. Pehling, Phys. Lett. A **146**, 199 (1990).
[12] P. W. O'Connor, J. Gehlen, and E. Heller, Phys. Rev. Lett. **58**, 1296 (1987).
[13] *Handbook of Mathematical Functions,* Natl. Bur. Stand. Appl. Math. Ser. No. 55, edited by M. Abromowitz and I. A. Stegun (U.S. GPO, Washington, DC, 1964).
[14] In our case the eigenvalue Λ is positive. We believe our results are indicative of what would happen in general for unstable periodic orbits with positive eigenvalues.